International Journal of Nanomedicine

Dovepress
open access to scientific and medical research

Open Access Full Text Article

ORIGINAL RESEARCH

In situ fabrication of silver nanoparticle-filled hydrogen titanate nanotube layer on metallic titanium surface for bacteriostatic and biocompatible implantation

Zheng Wang[1]
Yan Sun[1]
Dongzhou Wang[2]
Hong Liu[2]
Robert I Boughton[3]

[1]Department of Cardiology, Heilongjiang Provincial Hospital, Haerbin, Heilongjiang, People's Republic of China; [2]State Key Laboratory of Crystal Materials, Shandong University, Jinan, People's Republic of China; [3]Department of Physics and Astronomy, Bowling Green State University, Bowling Green, OH, USA

Abstract: A silver nanoparticle (AgNP)-filled hydrogen titanate nanotube layer was synthesized in situ on a metallic titanium substrate. In the synthesis approach, a layer of sodium titanate nanotubes is first prepared on the titanium surface by using a hydrothermal method. Silver nitrate solution is absorbed into the nanotube channels by immersing a dried nanotube layer in silver nitrate solution. Finally, silver ions are reduced by glucose, leading to the in situ growth of AgNPs in the hydrogen titanate nanotube channels. Long-term silver release and bactericidal experiments demonstrated that the effective silver release and effective antibacterial period of the titanium foil with a AgNP-filled hydrogen titanate nanotube layer on the surface can extend to more than 15 days. This steady and prolonged release characteristic is helpful to promote a long-lasting antibacterial capability for the prevention of severe infection after surgery. A series of antimicrobial and biocompatible tests have shown that the sandwich nanostructure with a low level of silver loading exhibits a bacteriostatic rate as high as 99.99%, while retaining low toxicity for cells and possessing high osteogenic potential. Titanium foil with a AgNP-filled hydrogen titanate nanotube layer on the surface that is fabricated with low-cost surface modification methods is a promising implantable material that will find applications in artificial bones, joints, and dental implants.

Keywords: titanium implant, silver nanoparticle filling, ion substitution, bacteriostasis, cytocompatibility

Introduction

As a human body-friendly metal, titanium has been widely used for surgical instruments and implants, such as artificial bones, dental implants, etc.[1–3] However, the smooth surface of metallic titanium implants is resistant to combining with natural bone to form a firm contact interface because of its lack of biocompatibility.[4] To improve the biocompatibility of metallic titanium and its alloys, the most efficient approach is to coat a second layer on the metal surface by physical or chemical methods. A calcium phosphate-based layer is one of the most important coating materials, because it possesses bone-inducing properties. However, the great difference in the thermal expansion coefficient between metallic titanium and calcium phosphate often causes great stress, and the coating easily peels off from the titanium substrate.[5,6] Titanate and TiO_2 are other important coatings for titanium implants, because they are easily coated onto the surface of the titanium substrate by different methods.[7] Because the thermal expansion coefficients of TiO_2 and metallic titanium are very close, about

Correspondence: Hong Liu
State Key Laboratory of Crystal Materials, Shandong University, 27 Shandanan Road, Jinan 250100, People's Republic of China
Tel +86 531 8836 2827
Fax +86 531 8836 2827
Email hongliu@sdu.edu.cn

submit your manuscript | www.dovepress.com
Dovepress
http://dx.doi.org/10.2147/IJN.S45742

8.5×10^{-6}°C^{-1} for metallic titanium[8] and 8.7×10^{-6}°C^{-1} for anatase,[9] the bonding strength of TiO_2 or titanate coating is much higher than that of other coatings.[10] Recently, TiO_2 and titanate nanostructures assembled on titanium have been considered for applications in biocompatible medical implants. Among these methods, a TiO_2 nanotube layer anodized onto the surface of a metallic titanium substrate is the most popular approach[11] because of its good biocompatibility. However, the anodization method is complex with some toxic hydrogen fluoride involved, and is not suitable for the preparation of nanotubes on complicatedly shaped implants. Therefore, chemical synthesis, especially the hydrothermal synthesis method of attaching TiO_2 or titanate nanostructures onto a titanium substrate becomes a promising methodology for fabricating biocompatible titanium implants. Nanobelts, nanomeshes, and nanotubes have been successfully synthesized on a metallic titanium substrate and have proved to be biocompatible and bioactive.[12,13]

Apart from the biocompatibility and bioactivity of titanium implants, infection due either to the formation of biofilms on the implant surface or to the compromised immune ability at the implant/tissue interface has attracted increasing attention among researchers.[4–9] Although the injection of antibiotics is sometimes effective for antibacterial effect during treatment, it is usually difficult to reduce the implant-associated infection with routine antibiotic treatment, because bacteria in the biofilm are more resistant to antimicrobial agents than their planktonic counterparts.[10,11] The ideal approach to reduce bacterial colonization of the biomaterial is to prevent the adhesion of bacterial cells to the surface.[9,10] Therefore, it is desirable to take advantage of any bacteriostatic ability of the implant in order to prevent postoperative infection.

Silver has been used as a nonspecific biocidal agent for many decades because, not only does it exhibit nontoxicity toward mammalian cells with a suitable dose, but it also disinfects a broad spectrum of bacterial and fungal species, including antibiotic-resistant strains.[11,14,15] Up to now, many attempts using physical methods have been made to fabricate silver nanoparticle (AgNP)-coated titanium or titanium alloy implants.[10,16–18] Although hybrid implants made using the above-mentioned physical methods inhibit bacterial adhesion and growth without weakening the activity of living cells,[16–18] it is difficult to control the silver ion (Ag ion) release because of the compact structure of the films. Alternatively, chemical methods have been used for the surface modification of titanium metal with silver. Most chemical methods are related to the assembly of AgNPs on the titanium surface with bridge molecules, or to the absorption of Ag ions onto a nanostructure on the titanium substrate surface. However, the AgNPs can be released from the connection site under the biodegrading effects of body fluid during medical treatment and harm the surrounding tissue. Therefore, a way to place AgNPs in contained biocompatible and bioactive nanostructures on titanium implant surfaces, and to ensure that the nanoparticles are nested in the nanostructures, would be a valuable approach to getting high-performance self-antibacterial titanium implants.

In this paper, we construct a unique hierarchical nanostructure in situ on the metallic titanium surface by using a hydrothermal treatment and follow-up solution absorption and reduction. First, a layer of hydrogen titanate nanotubes was synthesized by alkali-hydrothermal and then HCl treatment, because the surface nanotexture of titanate can enhance cell attachment, cell spreading, and differentiation in comparison with a smooth titanium surface.[19] This procedure facilitates the integration of the implant directly with the surrounding bone. Second, Ag ions are inserted into the nanotubes via a process of silver nitrate solution absorption. Finally, the Ag ions are reduced by glucose, leading to the in situ formation of AgNPs in hydrogen titanate nanotubes, a result that offers the capability of long-term Ag^+ release. This hierarchical nanostructure is therefore expected to be a promising implant that not only offers biocompatibility due to the porous nanonetwork architecture, but also exhibits relatively long-term bactericidal activity due to the AgNP-filled hydrogen titanate nanotube structure on the titanium substrate.

Material and methods

The chemicals and biological reagents used throughout this study were commercial products with no further purification. All kits were used according to the manufacturer's instructions except where otherwise stated.

Preparation of AgNP-filled hydrogen titanate nanotube layer on titanium foil surface

Titanium foils (99.7% Ti TA2, $7 \times 7 \times 0.8$ mm^3; Baoti Group Co, Ltd, Baoji, Shaanzi, People's Republic of China) were sequentially mechanically polished with water sandpaper (grades 400, 600, 800, and 1,000) and then successively ultrasonically cleaned with acetone, ethanol, and ultrapure water. Sodium titanate nanotube layers were prepared on the surface of the titanium foil by an alkali-hydrothermal reaction at 140°C.[20] Briefly, the as-polished titanium foil was immersed

in 20 mL of 10 mol/L NaOH aqueous solution in a 24 mL Teflon-lined autoclave, followed by hydrothermal treatment at 140°C for 16 hours. The treated foil was washed thoroughly with ultrapure water followed by ultrasonic irradiation for 2 minutes to remove those nanotubes that were loosely attached to the top layer. A sodium titanate nanotube layer on titanium foil was thus obtained. The above material was dipped in 0.1 mol/L HCl aqueous solution for 24 hours and then rinsed repeatedly with ultrapure water until the water pH dropped to 7 in order to obtain a hydrogen titanate nanotube layer on the titanate surface. The titanium foil sample with hydrogen titanate nanotube layer will be referred to as NT-Ti. The as-prepared NT-Ti was dried in a vacuum dryer at 50°C to evaporate water in the channels of the hydrogen titanate nanotubes. The dried NT-Ti was immersed in 0.1 mM silver nitrate solution under shaking at 100 rpm at 37°C for 12 hours. After removal from the solution, the samples were rinsed with ultrapure water to remove excess Ag ions adsorbed on the surface and at the interface between the nanotubes and then dried in air. A titanium foil with a $AgNO_3$-filled hydrogen titanate nanotube layer on the surface was obtained, which will be referred to as $AgNO_3$-NT-Ti. The as-obtained $AgNO_3$-NT-Ti sample was then immersed into 0.1 mM glucose solution for 12 hours in order to reduce the Ag^+ in the nanotubes to Ag^0. Subsequently, the samples were repeatedly rinsed with ultrapure water prior to drying in the dark. A foil with a AgNP-filled nanotube layer on the titanium foil surface was obtained and will be referred to as AgNP-NT-Ti.

Materials characterization

A field-emission scanning electron microscope (HITACHI S-4800; Hitachi Ltd, Tokyo, Japan) was used to observe the morphology of the samples, and a high-resolution transmission electron microscope (HRTEM, JOEL JEM 2100; JOEL, Tokyo, Japan) was used to characterize the microstructure of the nanotubes scraped from the surface of the NT-Ti and AgNP-NT-Ti specimens. The chemical composition and crystal structure of the samples were characterized with energy-dispersive X-ray spectroscopy (EDS, EMAX Energy EX-350; HORIBA Ltd, Kyoto, Japan), Raman spectroscopy (Jobin-Yvon HR 800; HORIBA Ltd) and X-ray photoelectron spectroscopy (ESCALAB 250; Thermo Fisher Scientific, Waltham, MA, USA). Ag^+ concentration in the liquid was measured with an X Series ICP-AES (Thermo Fisher Scientific).

Ag ion release test

To obtain reliable data, three parallel samples were used for all of the following characterization and property assessments, and the resulting data value was taken to be the average of the three original data measurements. Two types of samples, $AgNO_3$-NT-Ti and AgNP-NT-Ti, were immersed in 3 mL of phosphate-buffered saline (PBS) at 37°C. After immersion for fixed amounts of elapsed time, the Ag ion concentration in the solution was measured with an atomic absorption spectrophotometer (HITACHI 180-80; Hitachi Ltd) to determine the released concentration. To stimulate the dynamic process of Ag ion release in vivo, the buffer solutions were completely removed from the container for analysis with a Varian atomic absorption spectrophotometer against a standard solution at the end of 1 day, 2 days, 3 days, 4 days, 5 days, 6 days, 9 days, 11 days, 13 days, and 15 days elapsed time, and then replaced with fresh buffer solution for the next analysis time point.

Antimicrobial test

Gram-negative *Escherichia coli* DH5α (*E. coli*) was cultivated in Luria-Bertani (LB) broth (1% w/v tryptone, 0.3% w/v yeast extract, 0.5% w/v NaCl) under 200 rpm shaking at 37°C for 3 hours to assess the antimicrobial properties of the three samples, NT-Ti, $AgNO_3$-NT-Ti, and AgNP-NT-Ti. In the bactericidal rate test, the samples were individually soaked into the tubes containing 5 mL of *E. coli* suspension (~106 CFU/mL). After coincubation in a rotary shaker at 37°C for 24 hours, 100 μL of culture suspension from each tube was uniformly spread on the LB agar plates and the number of viable bacterial colonies was counted after incubation at 37°C for 24 hours. The bacterial suspension for the control sample was diluted by 4×10^3 times. To quantify antibacterial ability, the bactericidal rate was calculated based on the following equation[21]:

$$\text{Bactericidal rate}(\%) = \frac{N_{Control} - N_{sample}}{N_{Control}} \times 100\% \quad (1)$$

where $N_{Control}$ and N_{sample} correspond to the number of colonies counted in the agar plate.

Another typical assessment of the antibacterial property of a material is the zone inhibition test. In the zone of inhibition test, 100 μL of *E. coli* suspension (~10^6 CFU/mL) was uniformly spread over several LB agar plates. Different sterile samples (all with dimensions of $7 \times 7 \times 0.8$ mm^3, n = 2) were placed at the center of the plate prior to incubation at 37°C for 24 hours.

Cell culture

To evaluate the cytocompatibility of the nanostructure-modified titanium foils, mouse preosteoblast cell line

MC3T3-E1 was cultured in α-minimum essential medium containing 10% fetal bovine serum and 1% penicillin-streptomycin at 37°C in an atmosphere of 5% CO_2 at 95% humidity. The cultured cells were detached by 0.25% trypsinization and suspended in fresh culture medium prior to evaluation of the cytocompatibility of the surface-modified titanium samples. Approximately 40,000 cells were added to each sample and the cell behavior was subsequently studied after a fixed culture time.

As-synthesized samples were sterilized by 30 minute soaking in 75% ethanol, following by 30 minute ultraviolet exposure on both sides. After rinsing twice in sterile ultrapure water, different samples (n = 3) were placed in the 48-well plates and seeded with 500 μL of cell suspension containing ~4×10^4 cells. The culture medium was changed every 2 days to continuously supply nutrition for the cells.

Cell proliferation

A cell counting kit-8 (Dojindo Molecular Technologies, Inc, Kumamoto, Japan) was used for quantitative evaluation of cell viability on various samples after incubation for 1 day, 3 days, and 5 days (n = 3 for each sample), by monitoring the absorbance of the formed formazan product at 450 nm using a microplate reader (Multiskan MK3, Thermo Fisher Scientific).

Next, qualitative analysis of cell proliferation was carried out through an immunofluorescence measurement of the nuclei, after staining with propidium iodide (PI; Life Technologies, Carlsbad, CA, USA). Briefly, cell-loaded samples were cultured for 3 days and then gently rinsed with PBS (37°C). Subsequently, the cells were fixed with a 3.7% PBS solution of formaldehyde for 10 minutes, following by rinsing three times with PBS. They were then extracted with 0.1% Triton X-100 (Sigma-Aldrich, St Louis, MO, USA) for 5 minutes and blocked with PBS containing 1% bovine serum albumin (Sigma-Aldrich) for 30 minutes. After rinsing twice with water (pH = 7), the samples were stained with PI for 5 minutes, followed by rinsing three times with water (pH = 7) prior to examination under a confocal laser scanning microscope (Leica Microsystems, Wetzlar, Germany) at an excitation wavelength of 488 nm.

Cell adhesion and morphology

Cell morphology was observed by staining both the F-actin and nuclei of the cells cultured on the samples for 5 days to obtain visual evidence of cell proliferation on different samples. For immunofluorescence measurements of F-actin, the cell-loaded samples cultured for 3 days were fixed with 3.7% formaldehyde solution for 10 minutes, then extracted with 0.1% Triton X-100 (Sigma-Aldrich) for 5 minutes, blocked with PBS containing 1% bovine serum albumin (Sigma-Aldrich) for 30 minutes, and stained with phalloidin conjugated to Alexa Fluor 488 (Life Technologies). In addition, the nuclei of the cells on BMP-2 loaded GCF and HGCCS were counterstained with PI (Life Technologies) for visible localization and observation. The samples were examined at excitation wavelengths of 488 nm and 633 nm.

Total intracellular protein content and alkaline phosphatase activity

After 1 day of culturing, the osteogenic medium (a regular medium described in cell culture section, with the addition of 10 mM β-glycerol phosphate, 50 mg/mL L-ascorbic acid, and 10 nM dexamethasone) was substituted by the regular culture medium. After incubation on the three kinds of samples, pure titanium foil, NT-Ti and AgNP-NT-Ti for 1 day, 3 days, and 5 days, the total amount of intracellular protein content was assayed using a bicinchoninic acid protein assay kit (KeyGen Biotech) by measuring the absorbance of the reaction solution at 570 nm after intracellular protein release.

To further assess the bioactivity of the samples, the alkaline phosphatase (ALP) activity of cells cultured on the three samples for 7 day, 14 days, and 21 days was measured. As an index, ALP activity was measured by using an ALP activity assay kit (Wako Pure Chemical Industries, Ltd, Osaka, Japan) and normalized by the protein content of cells cultured on different samples. Five parallel replicas for each sample were analyzed.

Statistics analysis

The statistical analyses of all experimental data were performed by using SPSS version 13.0 (SPSS, Inc, Chicago, IL, USA). Data were reported as means and standard deviations. Statistical comparisons were performed by analysis of variance for multiple comparisons, and statistical significance was accepted at $P < 0.05$.

Results and discussion

Surface microstructure

The as-synthesized samples were characterized by SEM and HRTEM. Figure 1 shows SEM images of the NT-Ti and AgNP-NT-Ti surfaces, and transmission electron microscope (TEM) images of the nanotubes scraped from the sample surfaces. From the low-resolution SEM image (Figure 1A), we observe that the NT-Ti surface looks smooth. The EDS spectrum (Figure 1A, inset) illustrates that the primary

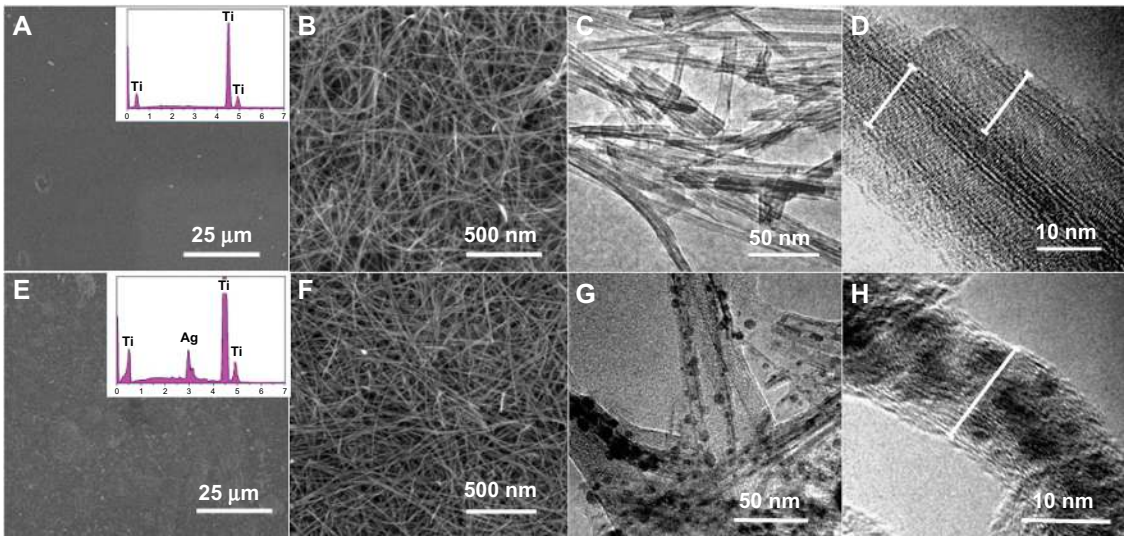

Figure 1 SEM and TEM images of NT-Ti and AgNP-NT-Ti surfaces.
Notes: (**A–D**) NT-Ti; (**E–H**) AgNP-NT-Ti.
Abbreviations: SEM, scanning electron microscope; TEM, transmission electron microscope; NT-Ti, titanium foil sample with hydrogen titanate nanotube layer; AgNP, silver nanoparticle; AgNP-NT-Ti; AgNP-filled nanotube layer on the titanium foil surface.

elemental constituent is titanium, and that no sodium can be found. The high-resolution SEM image of the NT-Ti surface shows a layer of wirelike nanostructures uniformly distributed on the sample surface (Figure 1B). The diameter of the wires is 10–12 nm, with lengths of up to several micrometers. Figure 1C shows a TEM image of the wirelike nanostructures scraped from the NT-Ti surface. From this image, we observe that the wirelike nanostructures are single crystalline nanotubes of about 10–12 nm in diameter. The HRTEM image of the sample further reveals the nanotube structure of the product. Combined with the EDS results, we conclude that the wirelike nanostructures appear to be $H_2Ti_3O_7$ nanotubes. The wall of the tube is composed of about two to three layers, a value that is consistent with the results of a similar approach to the synthesis of $H_2Ti_3O_7$ nanotubes on a Ti substrate.[22] The AgNP-NT-Ti surface is also smooth and similar to that of NT-Ti under low-resolution SEM observation (Figure 1E). The EDS spectrum (Figure 1E, inset) gives evidence that there is elemental silver on the surface of this sample. The high-resolution HRTEM image of AgNP-NT-Ti shows that the nanostructure of the sample still maintains a wirelike appearance, and no obvious difference can be found between the two samples (Figure 1F). The TEM image of AgNP-NT-Ti shows that the nanotubes still maintain their morphology, but there are some nanoparticles inside the nanotubes. Considering the EDS results for this sample, the nanoparticles are assumed to be silver-related nanoparticles. The HRTEM image of the nanotubes further indicates that the nanoparticles are located inside the tubes. From Figure 1F and H, we can find that the size of nanoparticles in hydrogen titanate nanotubes is from 3 to 8 nm, and the average diameter of the nanoparticles is about 5 nm. Between some bundled nanotubes, there are a few AgNPs outside of the nanotubes, because silver nitrate solution among the closed contacted bundled nanotubes is very difficult to be washed away. However, these nanoparticles are very tightly connected on the surface of the nanotubes, and difficult to be washed away even under ultrasonic irradiation. In addition, we found that most AgNPs outside the nanotubes can only be found at the bottom part of the nanotube film, because silver nitrate solution is absorbed on surface of the nanotubes; especially, the area among the bundled nanotubes in the bottom part of the nanotube film is more difficult to be washed away. However, because of the tight contact and the long path to the surface of the nanotube film, the nanoparticles in this area are difficult to split away from the surface of the nanotube to enter the cells and cause the cytotoxicity. In most cases, the nanoparticles, looking as if they are outside of the nanotubes, are actually located in the nanotube (see Figure S2). The fast growth of the nanocrystals makes the titanate walls of the nanotube distorted, and forms a bulge with a nanoparticle inside, which looks like the nanoparticle is located outside the nanotube under low-resolution TEM image. Because of the stress caused by different thermal expansion coefficients between the nanoparticles and the hydrogen titanate nanotubes, the crystallinity of the filled nanotube appears to be much lower than in the unfilled one.

Because the wall of the nanotube is very thin, and the thickness of $H_2Ti_3O_7$ nanotubes on the surface of titanium substrate is limited, it is difficult to get a diffraction peak for nanotubes on the samples. We tried several times to get an X-ray diffraction (XRD) pattern of the nanotubes on the surface of the samples, and only the diffraction pattern of metallic titanium can be checked out. To skirt this difficulty, we simulated the synthesis process by using titanium powder instead of titanium foil, and we got the pure titanate nanotube and Ag-NP-filled titanate nanotube samples without the metallic phase. The related result can be seen in Figure S1. The results proved that the nanotubes without AgNPs inside are single phase of $H_2Ti_3O_7$ with (200) plane preferentially, and AgNP-filled nanotubes possess two phases, $H_2Ti_3O_7$ and cubic metallic silver, which is consistent with the results from HRTEM and Raman.

Elements analysis

Raman spectra were taken on the samples to prove that the tubular nanostructures are $H_2Ti_3O_7$ nanotubes. Figure 2 shows the Raman spectra of NT-Ti and AgNP-NT-Ti. The spectrum of each sample possesses six broad peaks, at 120 cm^{-1}, 276 cm^{-1}, 440 cm^{-1}, 660–670 cm^{-1}, and 906 cm^{-1}, in good agreement with previous data on $H_2Ti_3O_7$.[23] The bands at 200 cm^{-1} and 906 cm^{-1} are intrinsic to the hydrogen titanate ($H_2Ti_3O_7$) phase and are suggested to be due to Ti–O–H.[23] The peak at 276 cm^{-1} is assigned to the characteristic phonon mode of the titanate nanotubes.[24] The peak at 440 cm^{-1}, according to the study of Ma et al,[25] is assigned to the Ti–O bending vibration involving six-coordinated titanium atoms and three-coordinated oxygen atoms. Based on the studies of Kasuga et al[26] and Sun and Li,[27] the peak at 660 cm^{-1} should be due to the Ti–O–Ti vibration in [TiO_6] octahedral layer in the titanate nanotubes. A very low and broad peak at 120 cm^{-1} shows that a very small amount of anatase exists in the sample (the typical peak of the anatase mode is at 144 cm^{-1}).

This result confirms that both nanotubes consist of hydrogen titanate, $H_2Ti_3O_7$.

Figure 3 reveals the X-ray photoelectron spectroscopy spectra of $AgNO_3$-NT-Ti and AgNP-NT-Ti. Two broad peaks at 368 eV and 374 eV for the $AgNO_3$-NT-Ti sample before glucose reduction are assigned to doublet $Ag_{3d5/2}$ and $Ag_{3d3/2}$ of the Ag^+ ions (Figure 3A).[28] After reduction (the AgNP-NT-Ti sample), the binding energy of the Ag 3d doublet exhibited 0.3 eV of blue shift (Figure 3B), which corresponds to Ag^0, according to the literature.[29] This observation confirms that Ag^+ was reduced to Ag^0 by glucose, and

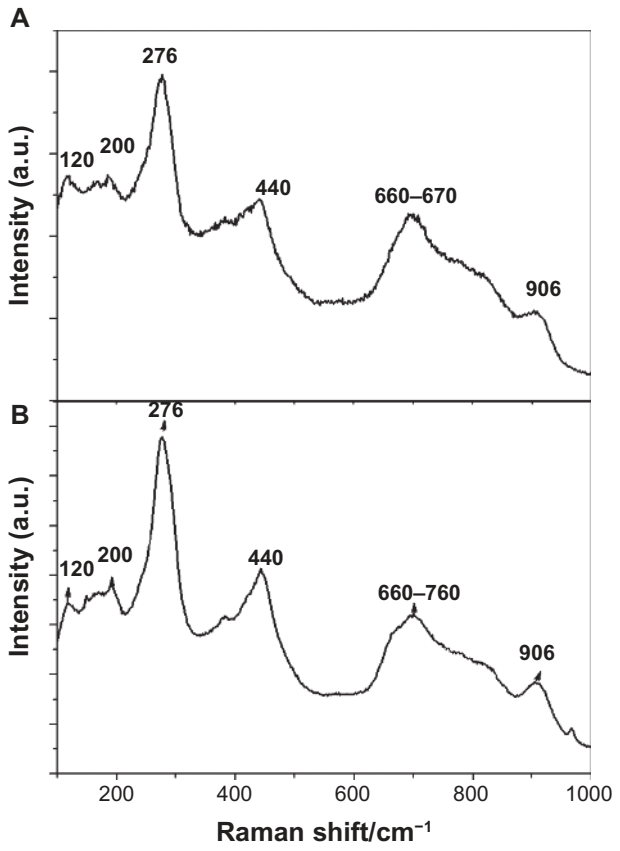

Figure 2 Raman spectra of NT-Ti and AgNP-NT-Ti.
Notes: (**A**) NT-Ti; (**B**) AgNP-NT-Ti.
Abbreviations: NT-Ti, titanium foil sample with hydrogen titanate nanotube layer; AgNP, silver nanoparticle; AgNP-NT-Ti; AgNP-filled nanotube layer on the titanium foil surface; a.u., arbitrary unit.

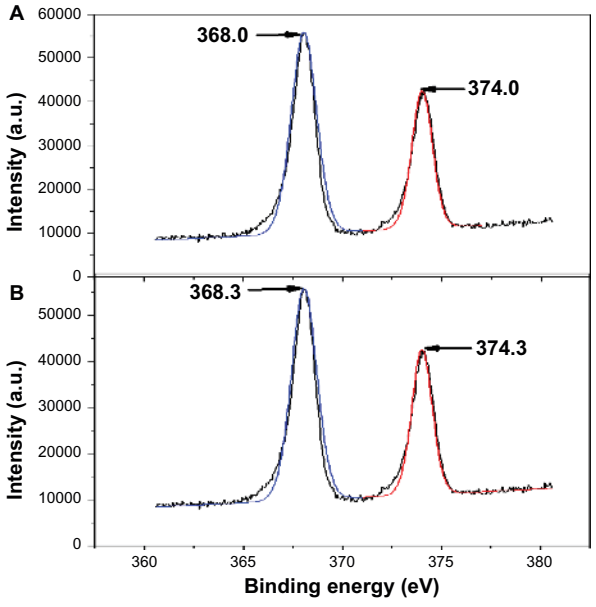

Figure 3 XPS spectra of $AgNO_3$-NT-Ti and AgNP-NT-Ti.
Notes: (**A**) $AgNO_3$-NT-Ti; (**B**) AgNP-NT-Ti.
Abbreviations: XPS, X-ray photoelectron spectroscopy; $AgNO_3$-NT-Ti, titanium foil with a $AgNO_3$-filled hydrogen titanate nanotube layer on the surface; AgNP, silver nanoparticle; AgNP-NT-Ti; AgNP-filled nanotube layer on the titanium foil surface; a.u., arbitrary unit.

that the nanoparticles in the $H_2Ti_3O_7$ nanotubes are metallic silver particles.

Ag ion release

Figure 4 shows the concentration of Ag ions released into PBS from the samples with increasing the immersion time. Two kinds of samples, $AgNO_3$-NT-Ti and AgNP-NT-Ti, exhibit different release properties. $AgNO_3$-NT-Ti releases Ag ions rapidly (Figure 4A). The accumulated released concentration increases very sharply with an increase in immersion time. On the fifth day, the accumulated concentration of Ag ions reaches approximately its highest value, and levels off to a stable constant value from the sixth to fifteenth day. AgNP-NT-Ti has a different Ag ion release behavior (Figure 4A). During the first 5 days, the accumulated released concentration of Ag ions for AgNP-NT-Ti is lower than that of $AgNO_3$-NT-Ti. Over the next few days, the released concentration keeps increasing until the fifteenth day. Figure 4B shows the daily Ag-ion release amount within the measurement period, in which one can see the different ion release characteristics for $AgNO_3$-NT-Ti and AgNP-NT-Ti. For $AgNO_3$-NT-Ti, in the first 5 days, the released amount stays at a very large value, but then drops to nearly zero on the seventh day. After the ninth day, no more Ag ions are released into solution, signaling the loss of antibacterial effect for this material. For the AgNP-NT-Ti sample, the daily ion released amount also decreases with an increase in immersion time, and the values of the daily released amount in the first 5 days are smaller than those of $AgNO_3$-NT-Ti. However, after 7 days, the daily released amount of the AgNP-NT-Ti sample stays at a constant asymptotic value, which ensures that the material maintains its antibacterial properties. On the fifteenth day, the daily released amount is greater than 0.02 mg/day.

The reason for the high Ag ion release rate in $AgNO_3$-NT-Ti is that the silver in the sample is in the ionic Ag^+ state, which can very easily diffuse into the surrounding solution when the sample is immersed in PBS. For AgNP-NT-Ti, the Ag^+ release is based on an oxidation process of AgNP.[30,31] When oxygen exists in the environment, the oxidization process of AgNPs occurs, and Ag ions can be released in the solution.

$$4Ag + O_2 + 2H_2O \rightarrow 4Ag^+ + 4OH^- \quad (2)$$

The Ag ion release rate of the AgNPs in the nanotubes is determined both by the dissolution rate (oxidization process) of the AgNPs and the diffusion rate. At first, the particles close to the open end of the nanotube are easily dissolved and diffuse into the surrounding solution, and so the release rate of Ag ions is very high. Over the next several days, AgNPs located in the inner part of the nanotube are more difficult to dissolve into the solution because of the restrictiveness of the nanotube walls, and so the Ag ion release rate is slowed down. These particular ion release characteristics give the AgNP-NT-Ti sample strong immediate bactericidal ability to combat the severe infection that often takes place immediately after surgery,[32] as well as long-term antibacterial ability to inhibit possible bacterial infection, which is an ideal property for titanium implants.

As shown in Figure 4B, after 15 days, the Ag ion released concentration for $AgNO_3$-NT-Ti has dropped to zero,

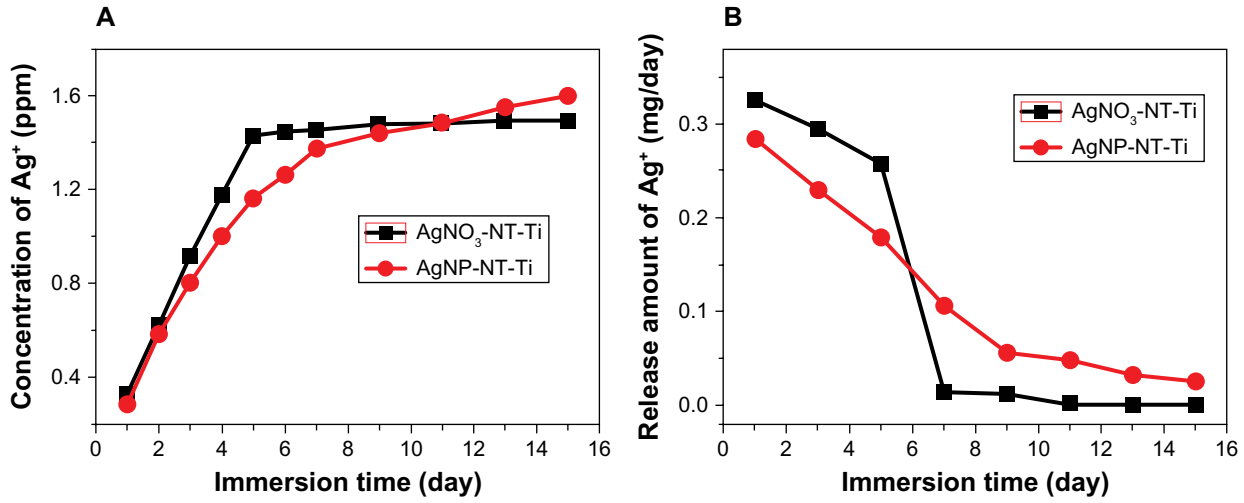

Figure 4 Concentration of silver ions released into PBS from the samples with increasing immersion time.
Notes: (**A**) Concentration of Ag^+ released. (**B**) Amount of Ag+ released.
Abbreviations: PBS, phosphate-buffered saline; $AgNO_3$-NT-Ti, titanium foil with a $AgNO_3$-filled hydrogen titanate nanotube layer on the surface; AgNP, silver nanoparticle; AgNP-NT-Ti; AgNP-filled nanotube layer on the titanium foil surface.

whereas, for AgNP-NT-Ti, it is still at a value of 50 ppb, which is much higher than the critical concentration level (0.1 ppb) or antimicrobial efficacy.[33,34]

Therefore, compared with $AgNO_3$-NT-Ti, AgNP-NT-Ti possesses a long-term Ag ion release capability that can induce a very efficient long-term antibacterial effect.

HRTEM observation of the AgNP-filled hydrogen titanate nanotubes got from the samples after immersion in PBS for 10 days and 15 days proved that the nanotubes can keep their tubelike morphology but the crystallinity decreases, and the small AgNPs dissolve and release away first, the larger ones can dissolve gradually, resulting in a longer time for Ag ion release (see Figure S3).

Antimicrobial properties

To evaluate the antimicrobial effectiveness of $AgNO_3$-NT-Ti and AgNP-NT-Ti, a tube test (n = 4) and a disk zone inhibition test (n = 4) were performed by using Ti foil and NT-Ti as control samples. Figure 5 shows the tube test results and disk zone inhibition test results. They show that both the $AgNO_3$-NT-Ti and AgNP-NT-Ti samples used for ion substitution led to very few colonies in the corresponding culture plates (Figure 5B and C). Moreover, the number of colonies was much less than that in the control sample, NT-Ti (Figure 6A). As a result, the tube test directly demonstrated that both sandwich nanostructures effectively inhibit bacteria growth. To quantify the tube test results, the bactericidal rates of $AgNO_3$-NT-Ti and AgNP-NT-Ti samples were 99.994% and 99.987%, respectively, which indicates that the samples exhibit very good bactericidal ability.

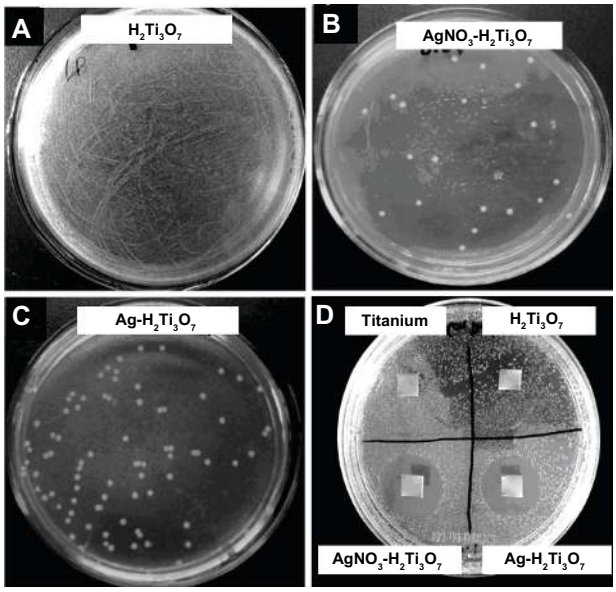

Figure 5 Tube test results and disk zone inhibition test results, A-D.

Figure 5D shows the results of the inhibition zone test for the $AgNO_3$-NT-Ti and AgNP-NT-Ti samples with titanium foil and NT-Ti as controls. It is well known that the size of the inhibition zone reflects the bacteriostatic ability of the sample. After incubation, obvious inhibition zones were found on both the $AgNO_3$-NT-Ti and AgNP-NT-Ti samples, while there were no inhibition zones on the two control samples. The diameter of the inhibition zones for the $AgNO_3$-NT-Ti and AgNP-NT-Ti samples is 23 mm and 21 mm, respectively. Therefore, the bactericidal property of the titanium foil sample with $AgNO_3$-filled $H_2Ti_3O_7$ nanotubes is slightly greater than that with AgNP-filled $H_2Ti_3O_7$ nanotubes after one day. A test of the long-term antibacterial properties of the $AgNO_3$-NT-Ti and AgNP-NT-Ti samples was performed by monitoring the release of silver for 15 days. An obvious inhibition zone (15 mm in diameter) was found around the AgNP-NT-Ti sample, but no inhibition zone was found for $AgNO_3$-NT-Ti. This result further demonstrates the long-term antibacterial capability of AgNP-NT-Ti.

Cytocompatibility assessment

AgNP-NT-Ti was selected for assessing cytocompatibility because of its potential applications in long-term self-sterilized bone implants. Titanium foil and NT-Ti are used as control samples for comparison.

Cell proliferation

One day after the cell seeding, the cell populations obtained on different samples were quite different (Figure 6). All the cell populations for the three samples increase with increasing culture time. After one day, the cell population on the NT-Ti surface is the largest, and the cell population on AgNP-NT-Ti is slightly lower, but at approximately the same value, which is twice the cell population on titanium foil. As proved by Ma et al[35] and Reno et al,[36] material surfaces containing –OH groups, which enhance cell adhesion by increasing surface hydrophilicity, have better cytocompatibility. In our study, $H_2Ti_3O_7$ is a layered tubular structure, and a large number of hydroxyl groups exist between the layers and on the nanotube surfaces. This property is the reason for the high cytocompatibility of the nanotube-contained nanostructures. By comparison with titanium foil, both samples, NT-Ti and AgNP-NT-Ti, possess similar outstanding cytocompatibility. This result indicates that the AgNPs in the $H_2Ti_3O_7$ nanotubes have no cytotoxicity because of the controlled release of Ag ions during cell

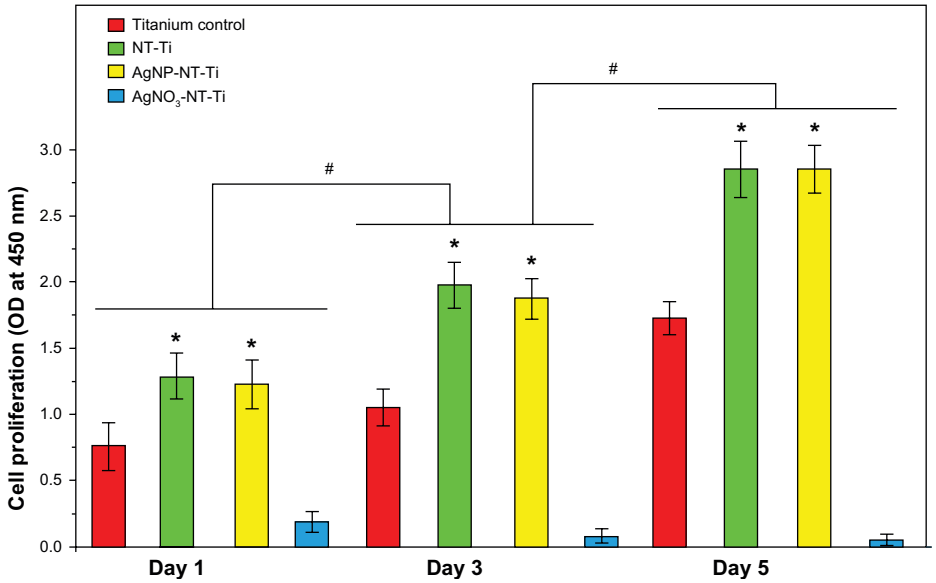

Figure 6 Cell proliferation for Day 1, Day 3 and Day 5, on titanium control, NT-Ti, AgNP-NT-Ti, and $AgNO_3$-NT-Ti.
Notes: Data are presented as mean plus standard deviation (n = 3, *$P < 0.05$, "0.01 mM" vs "Titanium"; #$P < 0.05$: the same sample vs the one at the previous time.
Abbreviations: NT-Ti, titanium foil sample with hydrogen titanate nanotube layer; AgNP, silver nanoparticle; AgNP-NT-Ti; AgNP-filled nanotube layer on the titanium foil surface; $AgNO_3$-NT-Ti, titanium foil with a $AgNO_3$-filled hydrogen titanate nanotube layer on the surface; OD, optical density.

culturing. In fact, the cytotoxicity of silver-related bactericides is often caused by too high an ion concentration and free nanoparticles that can enter the cells. In our study, the AgNPs are located in the $H_2Ti_3O_7$ nanotubes and cannot enter the cells directly, thus slowing down the ion release rate to a safe value.

After 3–5 days of culturing, the cell population for all three samples increases with increasing culturing time, and the optical density values of these three samples on the fifth day are twice as high as those measured on the first day. After 5 days of culturing, the number of living cells on both the NT-Ti and AgNP-NT-Ti samples is almost the same, but is about twice as much as on the titanium control sample. This result further demonstrates the high cytocompatibility of both NT-Ti and AgNP-NT-Ti. No cytotoxicity can be found in the AgNP-NT-Ti sample. However, for the sample $AgNO_3$-NT-Ti, a strong cytotoxic property arises. As mentioned above, the silver release rate from $AgNO_3$-filled nanotubes is higher than that from AgNP-filled nanotubes. Although the total release amount of Ag ions from $AgNO_3$-NT-Ti is slightly higher than that from AgNP-NT-Ti, the explosive release style of Ag ions from $AgNO_3$-NT-Ti causes great cytotoxicity compared with the slow release of Ag ions from AgNP-NT-Ti.

Considering the antibacterial test results as well, it can be inferred that the AgNP-NT-Ti samples are the best choice for building a self-sterilizing cytocompatible implant with compromised but strong bactericidal ability.

Cell morphology

Figure 8 shows the fluorescence images of the MC3T3-E1 cells cultured for 5 days on different samples: titanium control NT-Ti and AgNP-NT-Ti. The cell morphology for all the samples is polygonal, which is the characteristic shape of mouse preosteoblast cells. As shown in Figure 7B, 7E, and 7C, 7F, the cell density on NT-Ti and AgNP-NT-Ti is almost the same, and both are much larger than on titanium foil. This result indicates that $H_2Ti_3O_7$ can significantly enhance cell adhesion, cell migration, and final cell density on a sample surface, which is in agreement with the results from the cell proliferation experiments described above. This result also proves that AgNP-filled $H_2Ti_3O_7$ nanotubes do not give rise to cytotoxicity for MC 3T3-E1 cells, and that AgNP-NT-Ti possesses good self-sterilizing properties without cytotoxicity.

ALP activity

Figure 8 shows the ALP activity of the cells cultured on the NT-Ti, AgNP-NT-Ti, and titanium foil as control samples for 15 days and 21 days normalized to total protein concentration. After 7 days of culturing, the ALP activity of the two samples with nanotubes is plotted versus culturing time between the control and the "0.01 mM" samples at three chosen time points ($P > 0.05$). The ALP activity of the cells cultured on both two samples, NT-Ti and AgNP-NT-Ti, is higher than that for titanium foil. Although the ALP activity for all the three samples increases with increasing culturing time, after 15 days and 21 days have elapsed, the ALP activity for both

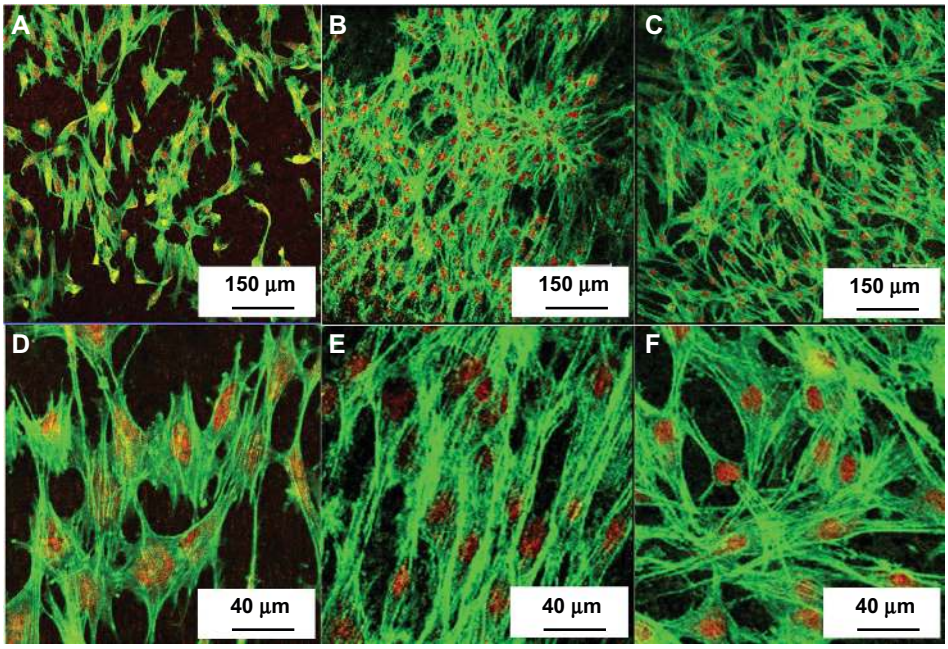

Figure 7 Fluorescence images of the MC3T3-E1 cells cultured for 5 days on titanium control, NT-Ti, and AgNP-NT-Ti.
Notes: (**A** and **D**) Titanium control. (**B** and **E**) NT-Ti. (**C** and **F**) AgNP-NT-Ti.
Abbreviations: NT-Ti, titanium foil sample with hydrogen titanate nanotube layer; AgNP, silver nanoparticle; AgNP-NT-Ti; AgNP-filled nanotube layer on the titanium foil surface.

two samples, NT-Ti and AgNP-NT-Ti, is the same value, which is about twice that for titanium foil after 21 days.

As is well known, ALP is an osteoblastic metabolic enzyme involved in mineral deposition and is an early marker of osteoblastic differentiation. ALP activity represents the osteoblast differentiation ability and osteogenic potential of MC-3T3-E1 cells.[37] Therefore, compared with titanium, titanium foil with an $H_2Ti_3O_7$ layer on the surface can enhance the differentiation of preosteoblast cells. As reported by Park et al[38] and Keselowsky et al,[39] hydroxyl (–OH) and amine ($–NH_2$) groups on a material surface can greatly enhance osteoblast differentiation. The existence of rich hydroxyl groups on the surface of $H_2Ti_3O_7$ nanotubes is the main reason for the enhancement of osteoblast differentiation of MC 3T3-E1 cells in this work. Most importantly, AgNPs located in the $H_2Ti_3O_7$ nanotubes do not decrease the tendency for the osteoblast differentiation of MC 3T3-E1 cells, which indicates that AgNP-NT-Ti possesses very desirable properties for applications to self-sterilizing implants including good cytocompatibility, long-term antibacterial properties, and high osteogenic potential.

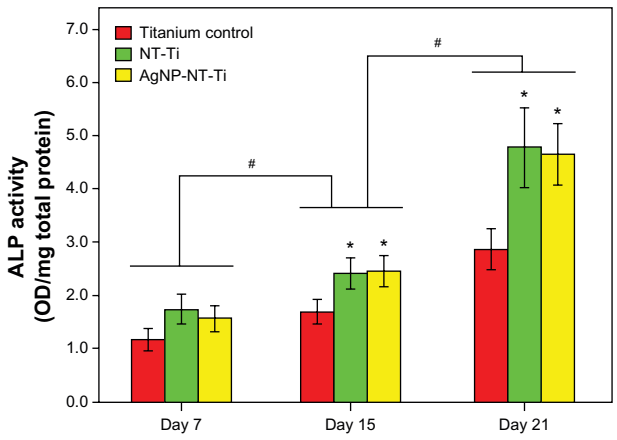

Figure 8 Alkaline phosphatase activity of the cells cultured on titanium control, NT-Ti, and AgNP-NT-Ti.
Notes: Data are presented as mean standard deviation (n = 3, $^*P < 0.05$, "0.01 mM" versus "Titanium"; $^\#P < 0.05$: the same sample versus the one at the previous time.
Abbreviations: NT-Ti, titanium foil sample with hydrogen titanate nanotube layer; AgNP, silver nanoparticle; AgNP-NT-Ti; AgNP-filled nanotube layer on the titanium foil surface; ALP, alkaline phosphatase; OD, optical density.

It is also well known that both Ag ions and AgNPs possess high bactericidal capability. The bactericidal activity of Ag ions is caused by their strong binding affinity to electron donor groups in biological molecules containing sulfur, oxygen, or nitrogen.[40–42] The antibacterial activity of AgNPs originates both from the release of Ag ions and from the nanoparticle itself. The nanoparticles attach onto the cell membrane, penetrate into the bacterium, and then bind to the deoxyribonucleic acid (DNA) or the -S-H on functional proteins to prevent replication.[42–44] Normally, for animal cells, AgNPs are more easily bonded with DNA and cause cytotoxicity because there is no cell wall on the surface of animal cells.[30] However, the results of our experiment

suggest that the titanium with AgNP-filled $H_2Ti_3O_7$ nanotube layer shows good cytocompatibility as well as bacteriostasis. A reasonable explanation for this dual function is that eukaryotic cells are usually larger than prokaryotic cells and exhibit a far bigger target for the attacking Ag ions. Eukaryotic cells also show higher structural and functional redundancy compared with prokaryotic cells. Therefore, a higher concentration of Ag^+ is required to achieve comparable toxic effects in eukaryotic cells than in bacterial cells. This difference provides a "therapeutic window" in which bacterial cells are successfully attacked, whereas harmful effects on eukaryotic cells have not yet been observed. The Ti implants with AgNP-filled $H_2Ti_3O_7$ nanotube layers on them used in our study take full advantage of the different responses to the AgNPs between bacteria and animal cells, and have good antibacterial ability in the absence of cytotoxicity. In addition, because the synthesis process is carried out in solutions without the involvement of any toxic chemicals, Ti implants with AgNP-filled $H_2Ti_3O_7$ nanotube layers on the surface will likely have applications in medical apparatus such as artificial bones, joints, and dental implants.

Conclusion

A AgNP-filled hydrogen titanate nanotube layer has been synthesized in situ on a Ti foil surface by an alkaline hydrothermal HCl immersion process, and subsequent absorption of silver nitrate, followed by reduction of Ag into AgNPs in glucose solution. AgNP-filled $H_2Ti_3O_7$ nanotube-layered titanium foils have a high bacteriostatic rate of 99.99% and possess long-term Ag ion release capability. At the same time, titanium foil with AgNP-filled $H_2Ti_3O_7$ nanotube layers on the surface was determined to have excellent cytocompatibility and high osteogenic potential, compared with pure titanium. The long-term bactericidal function is caused by the AgNPs located in the $H_2Ti_3O_7$ nanotubes, which can release sufficient Ag ions for antibacterial action, even though no AgNPs escape from the nanotube channel. The excellent cytocompatibility and high osteogenic potential is due to abundant OH^- on the surface of the nanotubes. However, for $AgNO_3$-filled $H_2Ti_3O_7$ nanotube on titanium substrate without reduction, the explosive silver release style causes an obvious cytotoxicity. The present work demonstrates that a AgNP-filled $H_2Ti_3O_7$ nanotube coating endows the titanium with the dual utility of antibacterial activity and cell compatibility. Therefore, a Ti substrate with AgNP-filled $H_2Ti_3O_7$ nanotubes on the surface is a promising implantable biomaterial.

Acknowledgments

This research was supported by National Natural Science Foundation of the People's Republic of China (NSFDYS: 50925205).

Disclosure

The authors report no other conflicts of interest in this work.

References

1. Garvin KL, Hanssen AD. Infection after total hip arthroplasty. Past, present, and future. *J Bone Joint Surg Am*. 1995;77(10):1576–1588.
2. Schmalzried TP, Amstutz HC, Au MK, Dorey FJ. Etiology of deep sepsis in total hip arthroplasty. The significance of hematogenous and recurrent infections. *Clin Orthop Relat Res*. 1992;(280):200–207.
3. Schutzer SF, Harris WH. Deep-wound infection after total hip replacement under contemporary aseptic conditions. *J Bone Joint Surg Am*. 1988;70(5):724–727.
4. Zimmerli W, Trampuz A, Ochsner PE. Prosthetic-joint infections. *N Engl J Med*. 2004;351(16):1645–1654.
5. Gristina AG, Oga M, Webb LX, Hobgood CD. Adherent bacterial colonization in the pathogenesis of osteomyelitis. *Science* 1985;228(4702):990–993.
6. Oakes JA, Wood AJJ. Infections in surgery. *N Engl J Med*. 1986;315:1129–1138.
7. Stewart PS, Costerton JW. Antibiotic resistance of bacteria in biofilms. *Lancet*. 2001;358(926):135–138.
8. Zhao L, Chu PK, Zhang Y, Wu Z. Antibacterial coatings on titanium implants. *J Biomed Mater Res B Appl Biomater*. 2009;91(1):470–480.
9. Navarro M, Michiardi A, Castaño O, Planell JA. Biomaterials in orthopaedics. *J R Soc Interface*. 2008;5(27):1137–1158.
10. Sittig C, Textor M, Spencer ND, Wieland M, Vallotton PH. Surface characterization of implant materials c.p.Ti, Ti-6 Al-7 Nb and Ti-6 Al-4V with different pretreatments. *J Mater Sci Mater Med*. 1999;10(1):35–46.
11. Agarwal A, Weis TL, Schurr MJ, et al. Surfaces modified with nanometer thick silver-impregnated polymeric films that kill bacteria but support growth of mammalian cells. *Biomaterials*. 2010;31(4):680–690.
12. Chi B, Victorio E S, Jin T. Synthesis of TiO_2-based nanotube on Ti substrate by hydrothermal treatment. *J Nanosci Nanotechol*. 2007;7(2):668–672.
13. Oh SH, Finõnes RR, Daraio C, Chen LH, Jin S. Growth of nano-scale hydroxyapatite using chemically treated titanium oxide nanotubes. *Biomaterials*. 2005;26(24):4938–4943.
14. Sambhy V, MacBride MM, Peterson BR, Sen A. Silver bromide nanoparticles/polymer composites: dual action tunable antimicrobial materials. *J Am Chem Soc*. 2006;128(30):9798–9808.
15. Cao H, Liu X. Silver nanoparticles-modified films versus biomedical device-associated infections. *Wiley Interdiscip Rev Nanomed Nanobiotechnol*. 2010;2(6):670–684.
16. Chen W, Liu Y, Courtney HS, et al. In vitro anti-bacterial and biological properties of magnetron co-sputtered silver-containing hydroxyapatite coating. *Biomaterials*. 2006;27(32):5512–5517.
17. Ewald A, Glückermann SK, Thull R, Gbureck U. Antimicrobial titanium/silver PVD coatings on titanium. *Biomed Eng Online*. 2006;5:22.
18. Cao H, Liu X, Meng F, Chub PK. Biological actions of silver nanoparticles embedded in titanium controlled by micro-galvanic effects. *Biomaterials*. 2011;32(3):693–705.
19. Bush JR, Nayak BK, Nair LS, Gupta MC, Laurencin CT. Improved bio-implant using ultrafast laser induced self-assembled nanotexture in titanium. *J Biomed Mater Res B Appl Biomater*. 2011;97(2): 299–305.
20. Wang YM, Du GJ, Liu H, Liu D, Qin SB, Wang N, Hu CG, Tao XT, Jiao J, Wang JY, Wang ZL, Nanostructured sheets of Ti-O nanobelts for gas sensing and antibacterial applications. *Adv Funct Mater*. 2008;18(7): 1131–1137.

21. Wang QF, Yu HJ, Zhong L, Liu JQ, Sun JQ, Shen JC. Incorporation of silver ions into ultrathin titanium phosphate films: in situ reduction to prepare silver nanoparticles and their antibacterial activity. *Chem Mater*. 2006;18(7):1988–1994.
22. Chatterjee S, Bhattacharyya S, Khushalani D, Ayyub P. Hydrothermally synthesized aligned arrays of self-assembled multiwalled hydrogen titanate nanotubes. *Cryst Growth Des*. 2010;10(3):1215–1220.
23. Rodríguez-González V, Obregón-Alfaro S, Lozano-Sánchez LM, Lee S-W. Rapid microwave-assisted synthesis of one-dimensional silver–H2Ti3O7 nanotubes. *J Mol Catal A Chem*. 2012;353–354:163–170.
24. Qian L, Du ZL, Yang SY, Jin ZS. Raman study of titania nanotube by soft chemical process. *J Mol Struct*. 2005;749:103–107.
25. Ma R, Fukuda K, Sakaki T, Osada M, Bando Y. Structural features of titanate nanotubes/nanobelts revealed by Raman, X-ray absorption fine structure and electron diffraction characterizations. *J Phys Chem B*. 2005;109(13):6210–6214.
26. Kasuga T, Hiramatsu M, Hoson A, Sekino T, Niihara K. Titania nanotubes prepared by chemical processing. *Adv Mater*. 1999;11(15):1307–1311.
27. Sun X, Li Y. Synthesis and characterization of ion-exchangeable titanate nanotubes. *Chemistry*. 2003;9(10):2229–2238.
28. Bates CW, Wertheim GK, Buchanan DNE. Nature of the 3.8 eV plasmon in x-ray photoemission from silver. *Phys Lett A*. 1979;72:178–180.
29. Wagner CD, Riggs WM, Davis LE, Moulders JF, Mullenberg GE. *Handbook of X-ray Photoelectron Spectroscopy: a Reference Book of Standard Data for Use in X-ray Photoelectron Spectroscopy*. Mullenberg GE, editor. Eden Prairie, MN: Perkin-Elmer Corporation; 1979.
30. AshaRani PV, Low Kah Mun G, Hande MP, Valiyaveettil S. Cytotoxicity and genotoxicity of silver nanoparticles in human cells. *ACS Nano*. 2009;3(2):279–290.
31. Choi O, Deng KK, Kim NJ, Ross L Jr, Surampalli RY, Hu Z. The inhibitory effects of silver nanoparticles, silver ions, and silver chloride colloids on microbial growth. *Water Res*. 2008;42(12):3066–3074.
32. Luo SH, Xiao W, Wei XJ, et al. In vitro evaluation of cytotoxicity of silver-containing borate bioactive glass. *J Biomed Mater Res B Appl Biomater*. 2010;95(2):441–448.
33. Kumar R, Münstedt H. Silver ion release from antimicrobial polyamide/silver composites. *Biomaterials*. 2005;26(14):2081–2088.
34. Joyce-Wohrmann RM, Munstedt H, Determination of the silver ion release from polyurethanes enriched with silver. Infection. 1999;27(1):46–48.
35. Ma Z, Gao C, Gong Y, Shen J. Chondrocyte behaviors on poly-L-lactic acid (PLLA) membranes containing hydroxyl, amide or carboxyl groups. *Biomaterials*. 2003;24(21):3725–3730.
36. Renò F, D'Angelo D, Gottardi G, et al. Atmospheric pressure plasma surface modification of poly(D,L-lactic acid) increases fibroblast, osteoblast and keratinocyte adhesion and proliferation. *Plasma Process Polym*. 2012;9(5):491–502.
37. Tenenbaum HC, Heersche JN. Differentiation of osteoblasts and formation of mineralized bone in vitro. *Calcif Tissue Int*. 1982;34(1):76–79.
38. Park JH, Olivares-Navarrete R, Wasilewski CE, Boyan BD, Tannenbaum R, Schwartz Z. Use of polyelectrolyte thin films to modulate osteoblast response to microstructured titanium surfaces. *Biomaterials*. 2012;33(21):5267–5277.
39. Keselowsky BG, Collard DM, Garcia AJ. Integrin binding specificity regulates biomaterial surface chemistry effects on cell differentiation. *Proc Natl Acad Sci U S A*. 2005;102(17):5953–5957.
40. Morones JR, Elechiguerra JL, Camacho A, et al. The bactericidal effect of silver nanoparticles. *Nanotechnology*. 2005;16(10):2346–2353.
41. Song HY, Ko KK, Oh LH, Lee BT. Fabrication of silver nanoparticles and their antimicrobial mechanisms. *Eur Cells Mater*. 2006;11:58.
42. Liao J, Anchun M, Zhu Z, Quan Y. Antibacterial titanium plate deposited by silver nanoparticles exhibits cell compatibility. *Int J Nanomedicine*. 2010;5:337–342.
43. Rai M, Yadav A, Gade A. Silver nanoparticles as a new generation of antimicrobials. *Biotechnol Adv*. 2009;27(1):76–83.
44. Darouiche RO. Anti-infective efficacy of silver-coated medical prostheses. *Clin Infect Dis*. 1999;29(6):1371–1377.

Supplementary materials

XRD characterization of the samples

Because it is very difficult to get the XRD pattern on the samples that the hydrogen titanate nanotube or AgNP-filled hydrogen titanate nanotube fill on the surface of the metallic titanium foil, we used metallic titanate particles to simulate the reaction between NaOH and titanium, the following ion substitution, and the reduction of silver ions in the nanotube. Because there is no interference of the Ti substrate, after very careful measurement, we have obtained the XRD pattern of $H_2Ti_3O_7$ nanotubes and AgNP-filled $H_2Ti_3O_7$ nanotubes (Figure S1).

From Figure S1A, we found that the peaks of $H_2Ti_3O_7$ (JCPDS card 41-192) are weak and broad, which indicates that the size of the nanotube is very small. The peak (200) is much higher than the other peaks of $H_2Ti_3O_7$, which demonstrates that the layer-structured wall of the nanotube grows along the (200) plane. From Figure S1B, we found that there is a very broad peak indexed to cubic Ag (111), which indicates that there are some very small silver nanoparticles in the sample. In addition, the (200) peak of $H_2Ti_3O_7$ becomes very broad, which is probably because of the distortion of the nanotube caused by the formation of AgNPs in the nanotube.

In summary, the results proved that the nanotubes without AgNPs inside are single phase of $H_2Ti_3O_7$ with (200) plane preferentially, and AgNP-filled nanotubes possess two phases, $H_2Ti_3O_7$ and cubic metallic silver.

Abnormal morphology of AgNP-filled hydrogen titanate nanotubes

In Figure S2, we found that some AgNPs are filled in the titanate nanotube. The nanoparticles are different sizes. The fast growth of the nanocrystals makes the titanate walls of the nanotube distorted, and a bulge forms with a nanoparticle inside, which looks as if the nanoparticle is located outside the nanotube under low-resolution TEM image.

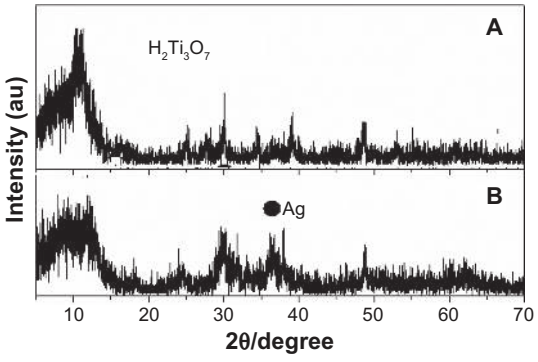

Figure S1 XRD patterns of $H_2Ti_3O_3$ nanotube and AgNP-filled titanium nanotubes.
Abbreviations: XRD, X-ray diffraction; AgNP, silver nanoparticle; au, arbitrary unit.

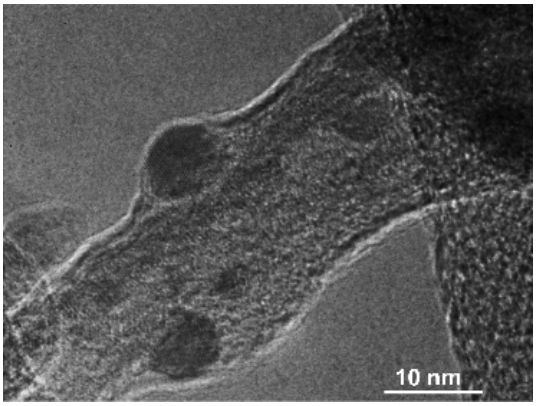

Figure S2 AgNP-filled hydrogen titanate nanotubes.
Abbreviation: AgNP, silver nanoparticle.

The nanotubes stripped from the samples after being soaked in PBS for 10 and 16 days were used to check the morphology variation of the nanotubes, and the nanoparticles inside (see Figure S3). HRTEM observation proved the nanotubes are keep in their tubelike morphology, but the crystallinity became lower, which is likely caused by the formation and stress release of the tube walls. For the 16 day immersed samples, it is difficult to find the nanoparticles in the nanotubes, which indicates that most of the AgNPs dissolved totally. For the samples immersed in PBS for 10 days, the small nanoparticles cannot be found in the nanotubes, but some big ones can be found inside the tube, and the crystallinity became very poor. This indicates that the small AgNPs could be dissolved and diffused out of the nanotubes first, and the larger AgNPs could be dissolved gradually and keep releasing Ag^+ for a longer time.

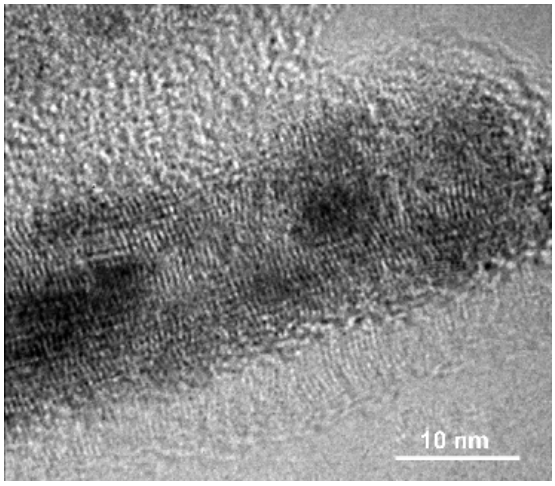

Figure S3 HRTEM of AgNP-filled hydrogen titanate nanotubes after 10 days silver release.
Abbreviations: HRTEM, high-resolution transmission electron microscope; AgNP, silver nanoparticle.